Supporting Information for

Rare Earth Pillars for Stabled Layered Birnessite Cathode Propelling Aqueous Zinc-Ion Batteries with Ultra-Long Cyclability

Jianwei Wang[a,b], Kangning Wang[b], Wenlin Zhang[b], Jinbo Zhang[b], Yanzhong Zhen[b], Feng Fu[b], and Yaping Du[a*]*

[a] J. Wang, Y. Du
Tianjin Key Lab for Rare Earth Materials and Applications
Center for Rare Earth and Inorganic Functional Materials
Haihe Laboratory of Sustainable Chemical Transformations
Smart Sensing Interdisciplinary Science Center
School of Materials Science and Engineering
National Institute for Advanced Materials
Nankai University
Tianjin 300350, China
E-mail: ypdu@nankai.edu.cn

[b] J. Wang, K. Wang, W. Zhang, J. Zhang, Y. Zhen, F. Fu
School of Chemistry & Chemical Engineering
Yan'an University
Yan'an 716000, China
E-mail: wkn1721@163.com

[*] Corresponding authors.

Experimental section

S1. Materials

Yttrium nitrate hexahydrate (AR, 99.5%) was purchased from Aladdin. $KMnO_4$ (AR, 99.5%) and hydrochloric acid (36–38%) were purchased from Xilong Scientific Co., Ltd. (China). Deionized water used in all experiments was purified through a Millipore system (18.25 MΩ).

S2. Synthesis of Y ions intercalation birnessite-MnO_2

Birnessite-MnO_2 and Y ions intercalation birnessite-MnO_2 were synthesized by a simple one-step hydrothermal method. In brief, (0, 0.1, 0.2, 0.3) mmol of $Y(NO_3)_3 \cdot 6H_2O$ were dissolved in deionized water (70 mL). After 5 minutes of stirring, 10 mmol of $KMnO_4$ was dissolved in the as-obtained homogeneous solution under stirring for 30 minutes. Then, 0.5 mL of hydrochloric acid (36-38%) was added to the above solution with another 30 minutes of stirring. Lastly, each solution was transferred into a 100 mL Teflon-lined stainless steel autoclave and heated at 60 °C for 12 hours. After the autoclave was cooled to room temperature, the precipitates were centrifuged, alternately washed with ethanol and deionized water several times, and dried in a vacuum oven at 60 °C for 12 hours.

S3. Material characterizations

X-ray diffraction (XRD) pattern was collected on a Bruker D8 Advance diffractometer (Cu Kα, λ=0.15418 nm, Germany). The morphology and microstructure of the samples were observed by field emission scanning electron microscope (SEM) (S4801-IM, Japan), transmission electron microscope (TEM) with energy dispersive X-ray spectroscopy (EDS) capabilities (FEI Tecnai G2 F20, USA). The Raman spectrum was obtained by In Via Reflex (λ=785 nm, UK). The surface elemental constituent and chemical valence states were analyzed by X-ray photoelectron spectroscopy (XPS) (Thermo Fisher, USA). The thermogravimetric (TG) of the samples was tested by TG-DSC 3 (Mettler, Switzerland). The element contents of the as-prepared materials were determined by Inductive Coupled Plasma Emission Spectrometer (ICP) (Aglient-5110, USA).

S4. Electrochemical measurement

To make a slurry, thoroughly mix the active ingredient, conductive agent (Super P), and binder (polyvinylidene fluoride) in N-methyl-2-pyrrolidone at a mass ratio of 7:2:1. Then, the obtained slurry was coated on titanium mesh and dried (60 °C, 12 hours) it for later use. Finally, the titanium mesh loaded with active materials is cut into numerous disk electrodes. The average mass loading of active material in each electrode was about 1-2 mg. The cycle performance and rate performance were measured using a battery tester (Wuhan LANHE, CT3002A, China) at a voltage of 0.8-1.8 V (vs. Zn^{2+}/Zn). On a CHI 660E electrochemical workstation (Shanghai Chenhua, China), cyclic voltammetry (CV) tests and electrochemical impedance

spectroscopy (EIS) experiments were performed. All electrochemical tests were measured under air at room temperature. Before the formal test, each cell was activated several cycles.

S5. First-Principles Calculations

All the theoretical simulations are calculated by DFT as implemented in Vienna ab initio simulation package (VASP).[1] The electron ion interactions were treated using the projection enhanced wave (PAW) pseudopotential. The Perdew Burke Ernzerhof (PBE) functional in Generalized Gradient Approximation (GGA) was adopted to describe the exchange-correlation effects.[2] The electronic and geometric relaxation were carried out with 4×3×2 Birnessite supercell, wherein, Y and K atoms as well as water molecules inserted between MnO_2 layers. The plane wave cutoff was set to be 450 eV, and the Brillouin zone was sampled with a 2×2×2 grids K-point for calculations. The structures were optimized with energy converged of 10^{-6} eV and force converged of 0.01 eV/Å for each atom.

S6. Galvanostatic Intermittent Titration Technique (GITT)

GITT test was carried out on $Y_{0.04}K_{0.16}Mn_2O_4 \cdot 2.3H_2O$ material at the current density of 0.1 A g^{-1} (**Figure S11**). The current pulse time and relaxation time were 5 min and 60 min, respectively. The diffusion coefficient can be calculated based on the equation (S1):

$$D_{Zn^{2+}} \approx \frac{4}{\pi\tau}\left(\frac{m_B V_m}{M_B S}\right)^2\left(\frac{\Delta Es}{\Delta E\tau}\right)^2 \quad \left(\tau \ll \frac{L^2}{DZn2+}\right)$$

where τ represents the duration of current pulse. L is equal to thickness of electrode. m_B, M_B and V_m represent the mass of active material, molecular weight (g/mol) and molar volume (cm^3/mol) respectively. S is the total contacting area of electrode with electrolyte. ΔE_S and ΔE_τ are the steady-state voltage change (V) by the current pulse and voltage change (V) during the constant current pulse (eliminating the voltage changes after relaxation time).

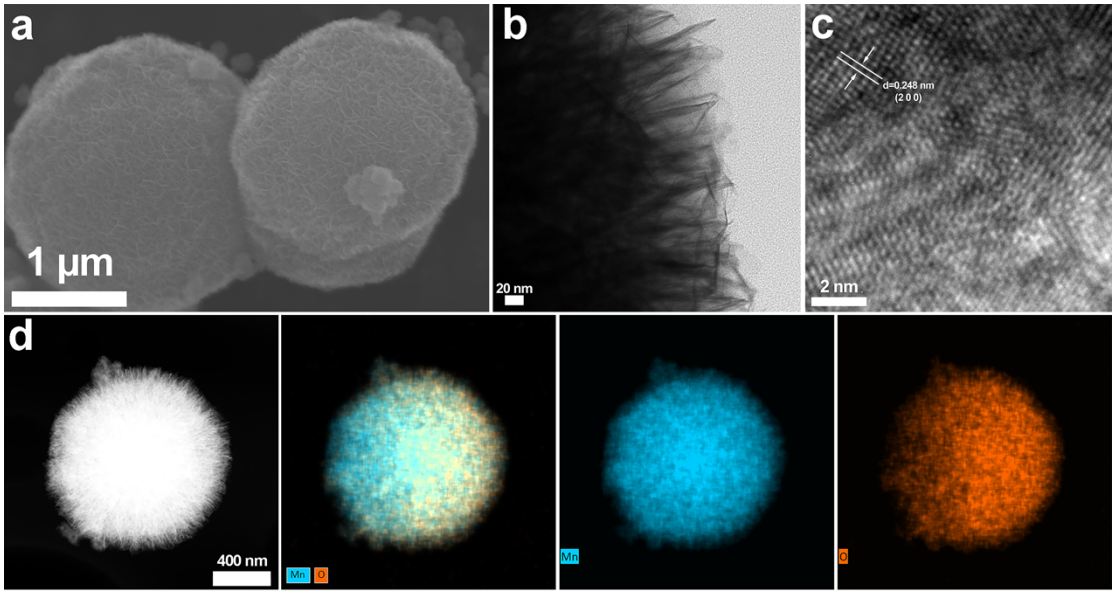

Figure S1. a) SEM image of $K_{0.24}Mn_2O_4 \cdot 1.9H_2O$. b, c) TEM images of $K_{0.24}Mn_2O_4 \cdot 1.9H_2O$. d) Elemental mapping images of $K_{0.24}Mn_2O_4 \cdot 1.9H_2O$.

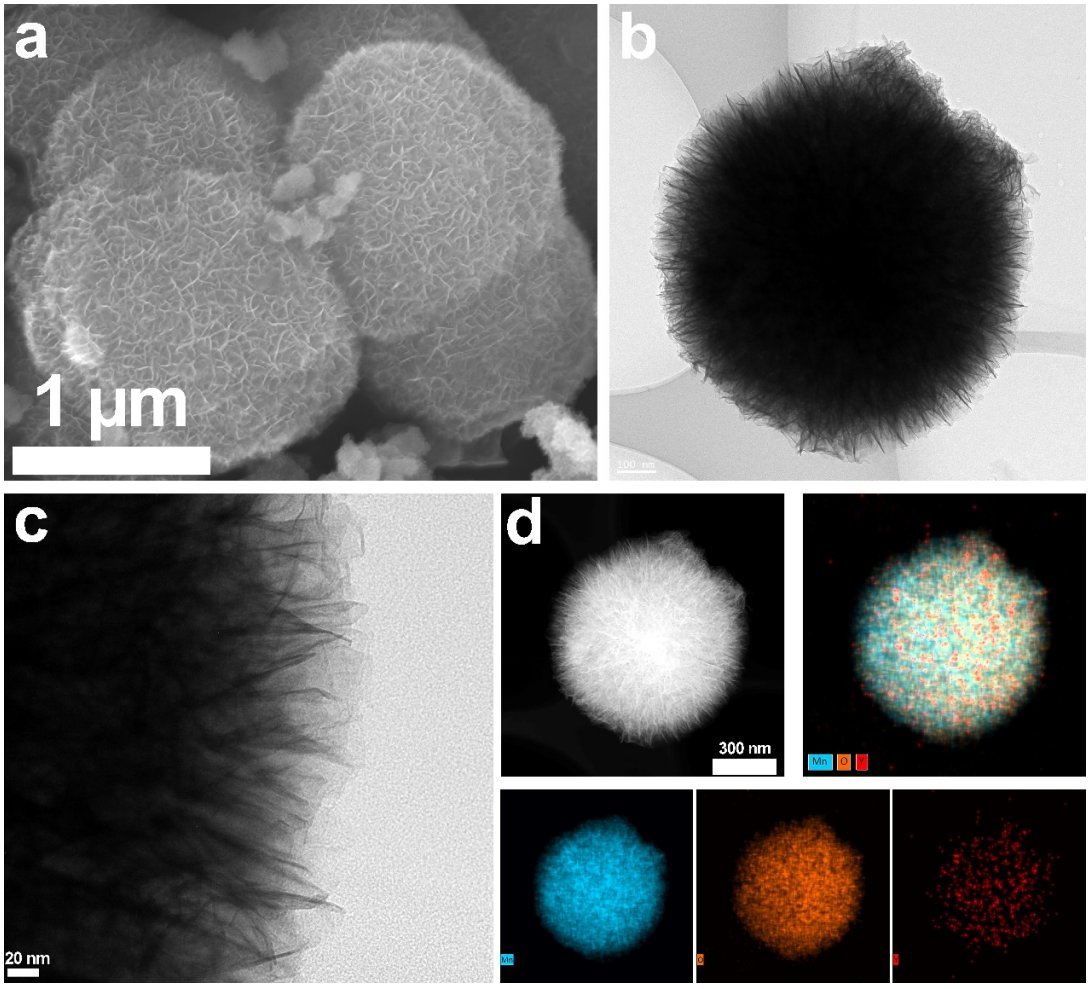

Figure S2. a) SEM image of $Y_{0.03}K_{0.19}Mn_2O_4 \cdot 2.2H_2O$. b, c) TEM images of $Y_{0.03}K_{0.19}Mn_2O_4 \cdot 2.2H_2O$. d) Elemental mapping images of $Y_{0.03}K_{0.19}Mn_2O_4 \cdot 2.2H_2O$.

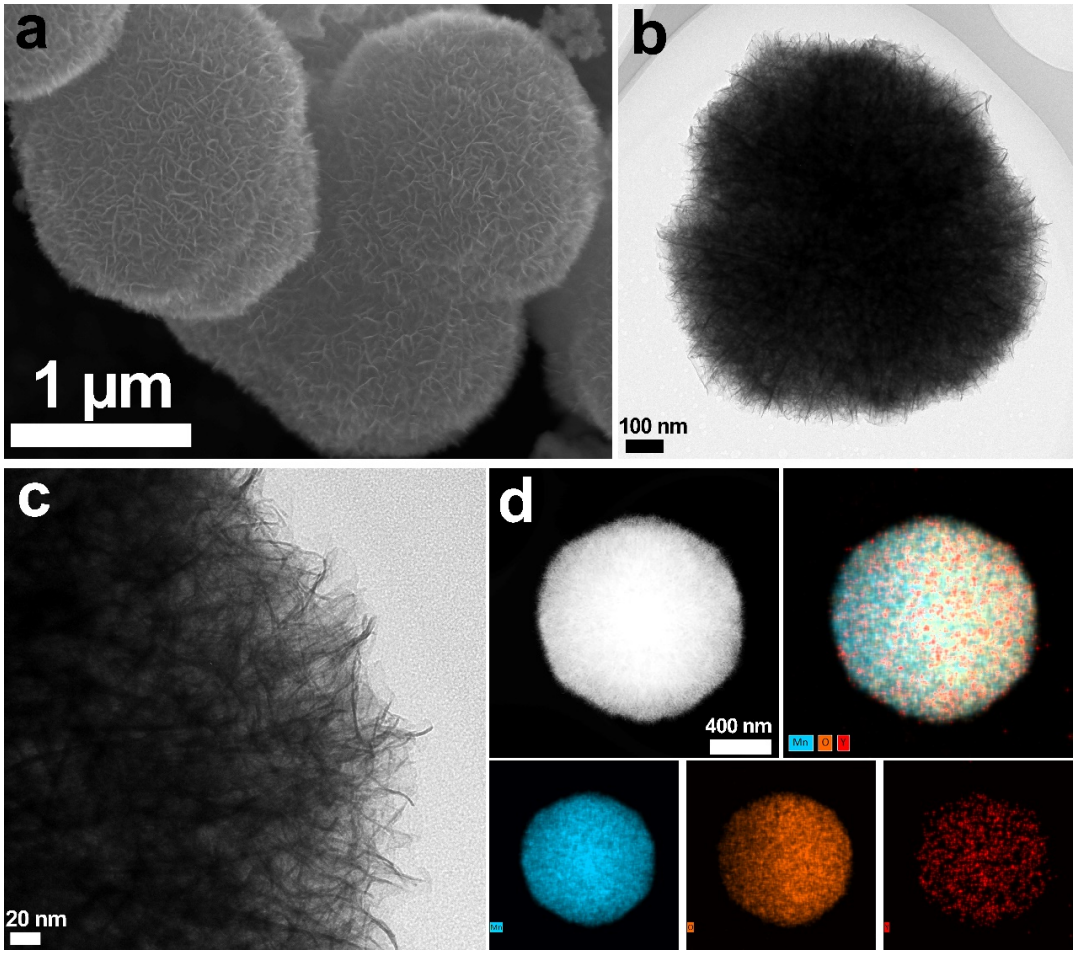

Figure S3. a) SEM image of $Y_{0.06}K_{0.15}Mn_2O_4 \cdot 2.4H_2O$. b, c) TEM images of $Y_{0.06}K_{0.15}Mn_2O_4 \cdot 2.4H_2O$. d) Elemental mapping images of $Y_{0.06}K_{0.15}Mn_2O_4 \cdot 2.4H_2O$.

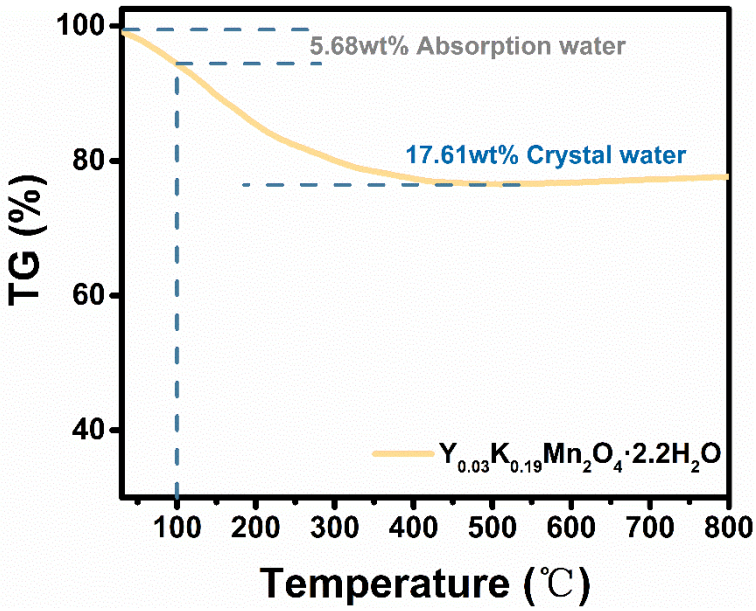

Figure S4. TG curve of $Y_{0.03}K_{0.19}Mn_2O_4 \cdot 2.2H_2O$.

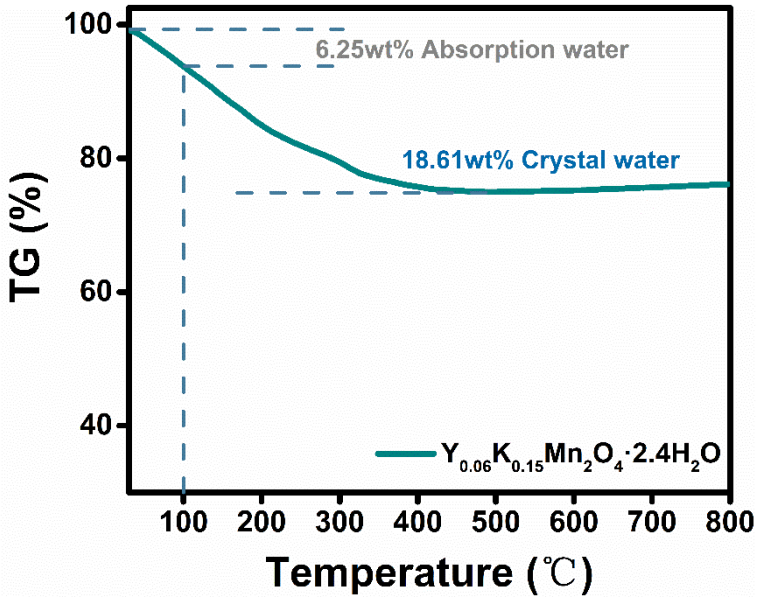

Figure S5. TG curve of $Y_{0.06}K_{0.15}Mn_2O_4 \cdot 2.4H_2O$.

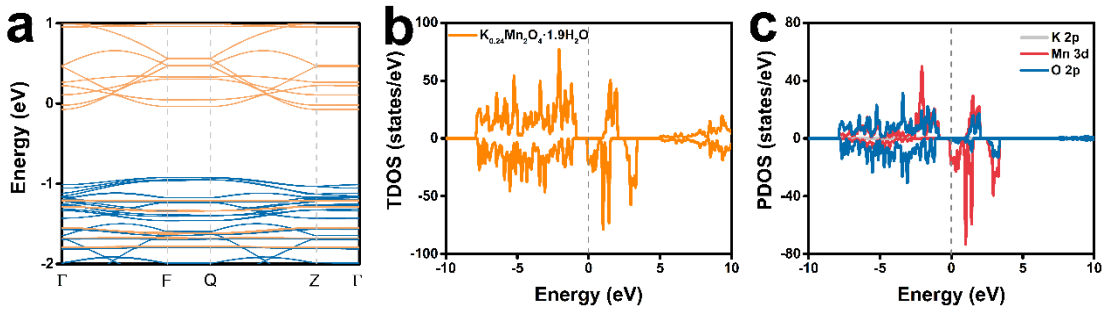

Figure S6. a-c) The calculated band structure, TDOS patterns, and PDOS patterns of $K_{0.24}Mn_2O_4 \cdot 1.9H_2O$.

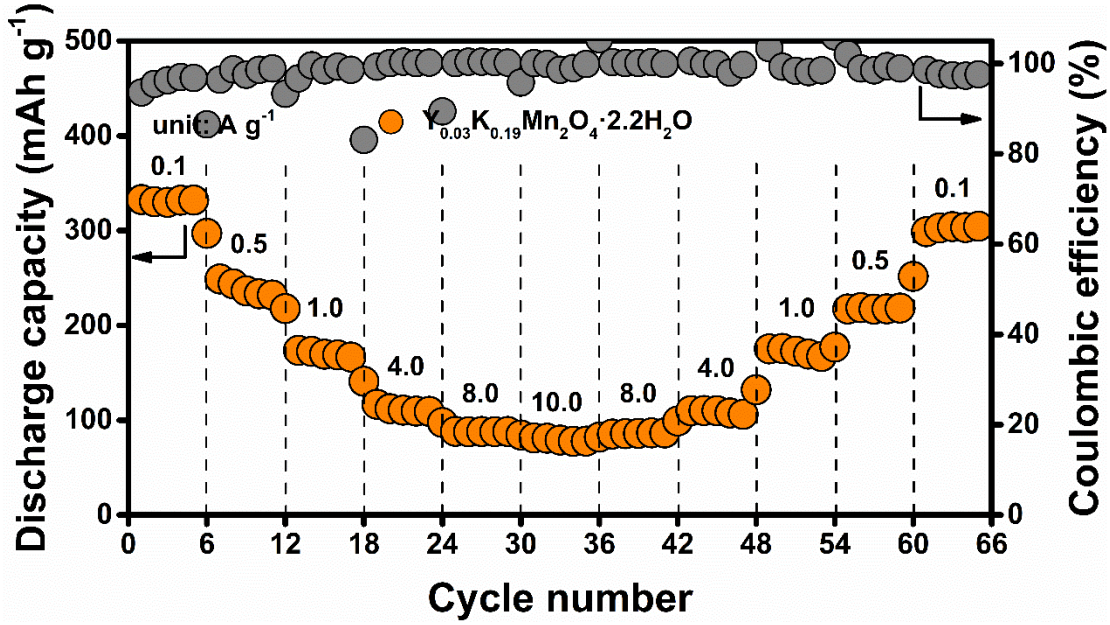

Figure S7. Rate performance of $Y_{0.03}K_{0.19}Mn_2O_4 \cdot 2.2H_2O$ at various current densities.

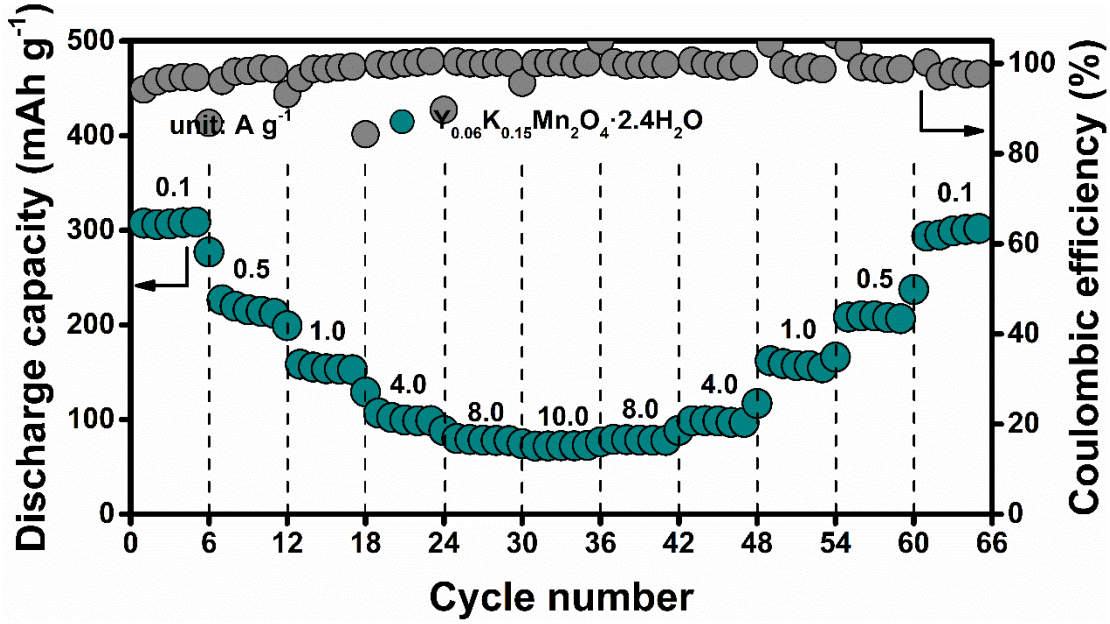

Figure S8. Rate performance of $Y_{0.06}K_{0.15}Mn_2O_4 \cdot 2.4H_2O$ at various current densities.

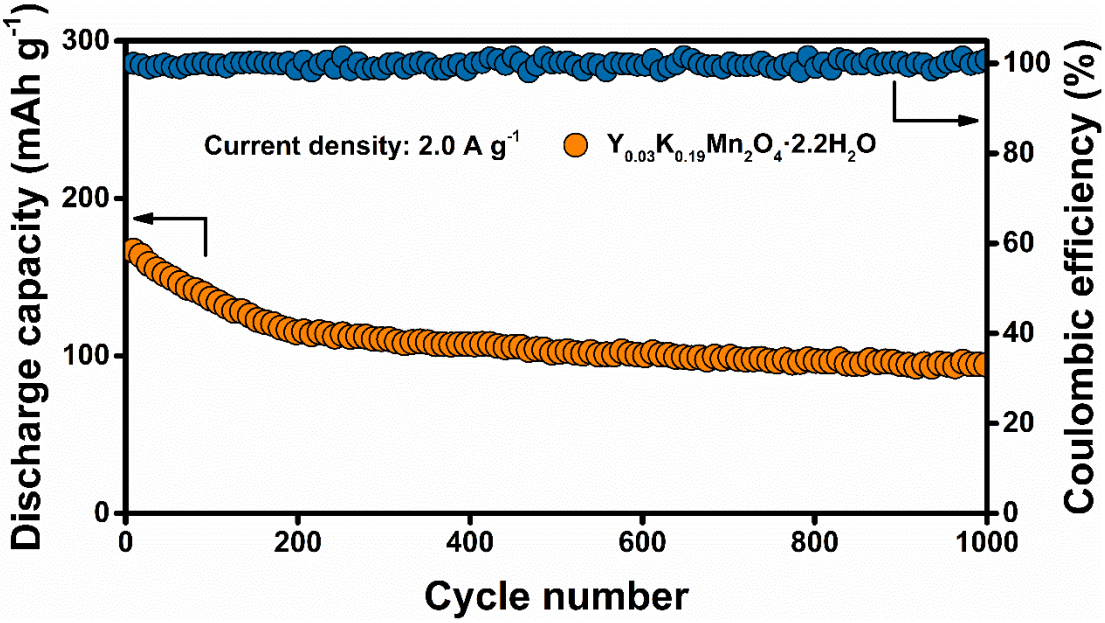

Figure S9. Cycle performance of $Y_{0.03}K_{0.19}Mn_2O_4 \cdot 2.2H_2O$ at 2.0 A g^{-1}.

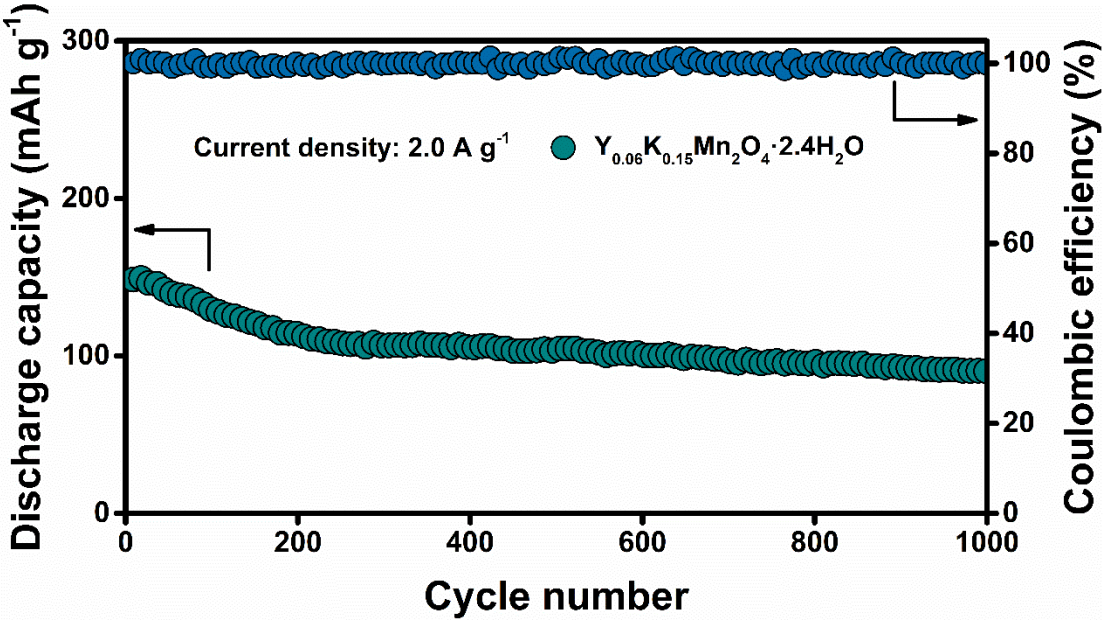

Figure S10. Cycle performance of $Y_{0.06}K_{0.15}Mn_2O_4 \cdot 2.4H_2O$ at 2.0 A g^{-1}.

Table S1. ICP analysis of the as-fabricated samples.

	Y (wt%)	Mn (wt%)	K (wt%)
$K_{0.24}Mn_2O_4 \cdot 1.9H_2O$	0%	40.9845%	3.5014%
$Y_{0.03}K_{0.19}Mn_2O_4 \cdot 2.2H_2O$	1.1135%	40.8052%	2.7650%
$Y_{0.04}K_{0.16}Mn_2O_4 \cdot 2.3H_2O$	1.4279%	39.8374%	2.2818%
$Y_{0.06}K_{0.15}Mn_2O_4 \cdot 2.4H_2O$	1.9276%	40.0475%	2.1765%

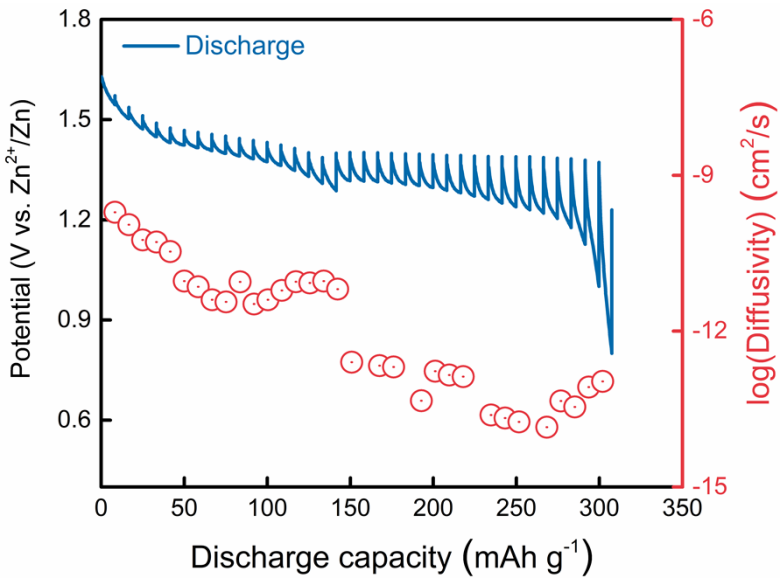

Figure S11. GITT profiles and ion diffusion coefficients of $Y_{0.04}K_{0.16}Mn_2O_4 \cdot 2.3H_2O$.

The results show that its diffusion coefficient (LogD) is between -13 cm^2/s and -10 cm^2/s. This high diffusion coefficient indicates that $Y_{0.04}K_{0.16}Mn_2O_4 \cdot 2.3H_2O$ material has excellent diffusion kinetics of zinc ions.

Table S2. Comparison of cathode performance in AZIBs between this work and previously reported.

Cathode material	Specific capacity (0.1 A g^{-1})	Cycle number	Ref.
$Y_{0.04}K_{0.16}Mn_2O_4·2.3H_2O$	**292.8 mAh g^{-1}**	**24,000 (8 A g^{-1})**	**This work**
$Mg_{0.9}Mn_3O_7·2.7H_2O$	N/A	5000 (5 A g^{-1})	[3]
BMO-6	363 mAh g^{-1}	10,000 (1 A g^{-1})	[4]
La-V_2O_5	405 mAh g^{-1}	10,000 (10 A g^{-1})	[5]
AMO	401.7 mAh g^{-1}	2000 (2 A g^{-1})	[6]
$(NH_4)_xWO_3$	153 mAh g^{-1}	2200 (5 A g^{-1})	[7]
K−V_2C@MnO_2	N/A	10,000 (5 A g^{-1})	[8]
δ-MnO_{2-x}−2.0	N/A	1500 (3 A g^{-1})	[9]
AMO	N/A	10,000 (4 A g^{-1})	[10]
MnO_2/MoO_3	333 mAh g^{-1}	16,000 (1 A g^{-1})	[11]

Table S3. The comparison of energy density of $Y_{0.04}K_{0.16}Mn_2O_4·2.3H_2O$ with the previously reported Zn-based systems.

Cathode material	Energy density	Ref.
$Y_{0.04}K_{0.16}Mn_2O_4·2.3H_2O$	**395.3 Wh kg^{-1} (135 W kg^{-1})**	**This work**
$Zn_3V_2O_7(OH)_2·2H_2O$	266 Wh kg^{-1} (66.5 W kg^{-1})	[12]
$Na_{0.44}MnO_2$	73.2 Wh kg^{-1} (181.5 W kg^{-1})	[13]
$Ca_{0.24}V_2O_5·0.83H_2O$	133 Wh kg^{-1} (1825 W kg^{-1})	[14]
VS_2	123 Wh kg^{-1} (32.3 W kg^{-1})	[15]
$Na_3V_2(PO_4)_2F_3$	97.5 Wh kg^{-1} (324 W kg^{-1})	[16]
$VO_2·xH_2O$	228 Wh kg^{-1} (135.3 W kg^{-1})	[17]
MnO_2	213.2 Wh kg^{-1} (768 W kg^{-1})	[18]

References

[1] G. Kresse, J. Furthmüller, *Physical Review B* **1996**, *54*, 11169-11186.

[2] J. P. Perdew, K. Burke, M. Ernzerhof, *Phys. Rev. Lett.* **1996**, *77*, 3865-3868.

[3] J. Li, N. Luo, L. Kang, F. Zhao, Y. Jiao, T. J. Macdonald, M. Wang, I. P. Parkin, P. R. Shearing, D. J. L. Brett, G. Chai, G. He, *Adv. Energy. Mater.* **2022**, *12*, 2201840.

[4] Y. Ma, M. Xu, R. Liu, H. Xiao, Y. Liu, X. Wang, Y. Huang, G. Yuan, *Energy Storage Materials* **2022**, *48*, 212-222.

[5] D. Zhang, J. Cao, Y. Yue, T. Pakornchote, T. Bovornratanaraks, J. Han, X. Zhang, J. Qin, Y. Huang, *ACS Appl. Mater. Interfaces* **2021**, *13*, 38416-38424.

[6] C. Chen, M. Shi, Y. Zhao, C. Yang, L. Zhao, C. Yan, *Chem. Eng. J.* **2021**, *422*, 130375.

[7] G. Tian, Q. Wang, Z. Qu, H. Yu, D. Zhang, Q. Wang, *Small* **2023**, *19*, 2206701.

[8] X. Zhu, Z. Cao, W. Wang, H. Li, J. Dong, S. Gao, D. Xu, L. Li, J. Shen, M. Ye, *ACS Nano* **2021**, *15*, 2971-2983.

[9] Y. Wang, Y. Zhang, G. Gao, Y. Fan, R. Wang, J. Feng, L. Yang, A. Meng, J. Zhao, Z. Li, *Nanomicro Lett.* **2023**, *15*, 219.

[10] H. Yao, H. Yu, Y. Zheng, N. W. Li, S. Li, D. Luan, X.-W. Lou, L. Yu, *Angew. Chem. Int. Ed.* **2023**, *62*, e202315257.

[11] Y. Liu, K. Wang, X. Yang, J. Liu, X.-X. Liu, X. Sun, *ACS Nano* **2023**, *17*, 14792-14799.

[12] C. Xia, J. Guo, Y. Lei, H. Liang, C. Zhao, H. N. Alshareef, *Adv. Mater.* **2018**, *30*, 1705580.

[13] T. Yuan, J. Zhang, X. Pu, Z. Chen, C. Tang, X. Zhang, X. Ai, Y. Huang, H. Yang, Y. Cao, *ACS Appl. Mater. Interfaces* **2018**, *10*, 34108-34115.

[14] C. Xia, J. Guo, P. Li, X. Zhang, H. N. Alshareef, *Angew. Chem. Int. Ed.* **2018**, *57*, 3943-3948.

[15] P. He, M. Yan, G. Zhang, R. Sun, L. Chen, Q. An, L. Mai, *Adv. Energy. Mater.* **2017**, *7*, 1601920.

[16] W. Li, K. Wang, S. Cheng, K. Jiang, *Energy Stor. Mater.* **2018**, *15*, 14-21.

[17] Z. Zhang, B. Xi, X. Wang, X. Ma, W. Chen, J. Feng, S. Xiong, *Adv. Funct. Mater.* **2021**, *31*, 2103070.

[18] Y. Liu, Y. Wang, X. Zhang, Y. Song, Y. Yi, H. Yin, Y. Zhu, G. Xu, Y. Zheng, *ACS Mater. Lett.* **2023**, *5*, 2820-2828.